ChemComm

ROYAL SOCIETY OF CHEMISTRY

FEATURE ARTICLE

View Article Online
View Journal

Cite this: DOI: 10.1039/d3cc03011c

Redox-active carborane clusters in bond activation chemistry and ligand design

Bryce C. Nussbaum, Amanda L. Humphries, Gayathri B. Gange and Dmitry V. Peryshkov *

Received 22nd June 2023,
Accepted 25th July 2023

DOI: 10.1039/d3cc03011c

rsc.li/chemcomm

Icosahedral *closo*-dodecaboranes have the ability to accept two electrons, opening into a dianionic *nido*-cluster. This transformation can be utilized to store electrons, drive bond activation, or alter coordination to metal cations. In this feature article, we present cases for each of these applications, wherein the redox activity of carborane facilitates the generation of unique products. We highlight the effects of exohedral substituents on reactivity and the stability of the products through conjugation between the cluster and exohedral substituents. Futher, the utilization of the redox properties and geometry of carborane clusters in the ligand design is detailed, both in the stabilization of low-valent complexes and in the tuning of ligand geometry.

Introduction

The activation of strong bonds has been the motivator of organometallic chemistry since the early development of transition metal catalysis. This reactivity largely stems from the combination of energetic and spatial features of filled and empty d-orbitals at a metal center, which influences its coordination environment and often leads to the ability to readily undergo two-electron cycling between oxidation states.[1]

Currently, significant attention is focused on the conceptually similar metal-free redox bond activation transformations inspired by recent discoveries.[2–19] It has been demonstrated that the electronic structure (*i.e.*, energy levels of frontier orbitals) of main group compounds can be significantly altered by changes in the substitution patterns or by the introduction of geometric constraints. As one prominent example, cyclic (alkyl)(amino)carbenes (CAACs), which possess both higher-energy HOMOs and lower-energy LUMOs than N-heterocyclic carbenes (NHCs), resulting in significantly greater σ-donation and π-acceptance, participate in the activation of strong H–H, B–H, Si–H, and N–H bonds through oxidative addition at the carbene center.[3,20,21] As another example, cycling between P(III) and P(V) states in geometrically constrained phosphorus compounds affords the possibility of oxidative addition and reductive elimination in a way that mimics the reactivity of transition metal complexes.[6,22–24]

The redox transformations in main group systems can be centered at a single atom (carbon or phosphorus atoms in the examples above), or they can occur through the participation of larger molecular fragments. The focus of this feature article is

Department of Chemistry and Biochemistry, University of South Carolina, 631 Sumter St, Columbia, South Carolina 29208, USA. E-mail: peryshkov@sc.edu

Bryce C. Nussbaum

Bryce Nussbaum received his bachelor's degree in chemistry in 2021 from Georgia Southern University. He is currently a graduate student at the University of South Carolina, working under Dmitry Peryshkov. His research interests include metallomimetic main group systems, metal-free bond activation, and frustrated Lewis pairs.

Amanda L. Humphries

Amanda Humphries received her bachelor's degree in chemistry from the University of South Carolina in 2020. She is currently pursuing a PhD degree in the Peryshkov Group at USC. Her research focuses on the synthesis and characterization of novel carboranyl phosphines, as well as reactivity studies towards potential applications in bond activation and catalytic transformations.

on the utilization of the redox activity of icosahedral *closo*-dicarbadodecaboranes ($C_2B_{10}H_{12}$, further referred to simply as "carboranes"), which are remarkably robust neutral molecular clusters with ten boron and two carbon vertices.[25,26] The electron delocalization within the cluster, which is related to the delocalized nature of planar aromatic rings, contributes to its high chemical stability.[27–29] These clusters have attracted increasing attention due to new applications in luminescent materials, batteries, medicine, ligand design, and catalysis.[30–41]

Neutral icosahedral $C_2B_{10}H_{12}$ cages are among the most studied examples of boron clusters. These carboranes are represented by three different isomers depending on the relative positions of the carbon atoms: *ortho*-, *meta*-, and *para*-$C_2B_{10}H_{12}$. During the past few decades, carborane chemistry has flourished due to its unique electronic, steric, and chemical properties. The unusually encumbered steric profile of the cluster is comparable to adamantane in van der Waals volume[42] and is further increased due to the presence of five neighboring cluster atoms adjacent to an exohedral bond in the icosahedral molecule.

Similarly to aromatic hydrocarbons, which feature delocalized bonding, the 3-D aromaticity of carborane involves extensive delocalized molecular orbitals.[27–29,43,44] The neutral carboranes possess a relatively low-energy LUMO that renders them reasonably strong electron acceptors amenable to electrochemical or chemical reduction.

The C–H bonds in carboranes are relatively acidic (pK_a is *ca.* 23), and as such can be deprotonated with strong bases, resulting in carbanions that can be utilized in reactions with organic or inorganic electrophiles, providing a major route for carbon vertex derivatization.[45,46] Factors driving the selectivity of carborane deprotonation and functionalization have been extensively studied.[47–49] The carbon atoms of *ortho*-$C_2B_{10}H_{12}$ form single bonds with exohedral substituents, and π-backdonation from those groups to the cluster can simultaneously increase the exohedral bond order and weaken the intracluster C–C bond.[50–52] There have been theoretical studies of the electronic and steric effects of exohedral substituents on this C–C bond length.[53,54] The electronic interaction between exohedral donor groups and the carborane cluster can be very significant, as evidenced by the recently disclosed structure of the diamine derivative 1,2-$(MesCH_2NH)_2$-$C_2B_{10}H_{10}$, which features one of the longest reported C–C bonds (1.931(3) Å, *cf.* 1.624(8) Å for the parent unsubstituted cluster).[55] Natural bond order (NBO) analysis attributed this extreme bond elongation to the efficient negative hyperconjugation between the lone pairs of the nitrogen atoms and the antibonding σ^*_{C-C} orbital in the *ortho*-carborane cluster.[56]

One feature, pertinent to this review, is the ability of the *ortho*-carborane, *closo*-$\{C_2B_{10}\}$, cluster to accept two electrons with conversion to the open *nido*-$\{C_2B_{10}\}$ isomer.[57,58] The cyclic voltammograms of *ortho*-$C_2B_{10}H_{12}$ and its derivatives often exhibit an unresolved two-electron reduction wave.[59–61] For instance, *ortho*-$C_2B_{10}H_{12}$ has been reported to undergo reduction to a dianion at a potential of −2.9 V *vs.* Fc^+/Fc.[62,63] Significant structural rearrangements occur during cluster opening upon reduction, causing a quasi-reversible or irreversible appearance of the cyclic voltammograms.[64] The structure of open-cage isomers that form upon reduction is much less studied, with only a few examples of isolated reduced clusters.[64] Exohedral substituents have been documented to have significant effects on the reduction potentials of carborane derivatives.[58] For example, the chemical reduction of unsubstituted *ortho*-$C_2B_{10}H_{12}$ with sodium metal produces the 7,9-$C_2B_{10}H_{12}^{2-}$ isomer that features an open six-membered ring face, while our results presented below show that the chemical reduction of carboranyl diphosphines affords a different, C_2-symmetric cage isomer (Fig. 1).[57,65] In addition, the outcome of cluster reduction depends on the reagent used, as

Gayathri B. Gange

Gayathri Gange began her education as an inorganic chemist in 2010 at the University of Colombo in Sri Lanka. She obtained her bachelor's degree (specialized in chemistry) in 2015 and then moved to South Carolina for her doctoral studies. She received her PhD degree in inorganic chemistry in 2022 from the University of South Carolina under the guidance of Dmitry Peryshkov, working on the synthesis and reactivity studies of novel carborane scaffolds. She is currently a Process Engineer at Intel Corporation in Oregon.

Dmitry V. Peryshkov

Dmitry Peryshkov started his independent career in 2013 at the Department of Chemistry and Biochemistry at the University of South Carolina, where he is currently an associate professor. He obtained an undergraduate degree in Materials Science from Moscow State University. In 2011, he earned a PhD degree at Colorado State University, under the supervision of Steven Strauss, working on polyfluorinated superweak anions. Following that, he was a postdoctoral researcher with Richard Schrock at Massachusetts Institute of Technology, working on tungsten oxo alkylidenes. The current group's research revolves around the redox chemistry of main group elements as well as transition metal catalysis.

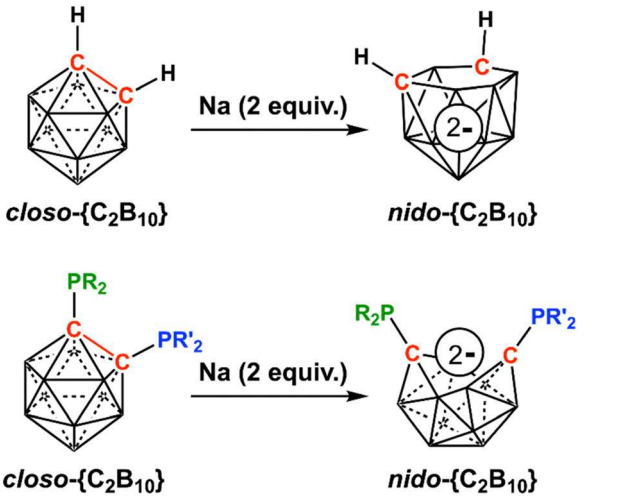

Fig. 1 Chemical reduction of *ortho*-carborane (top) and carboranyl diphosphines (bottom), highlighting the different *nido*-{C_2B_{10}} geometries.

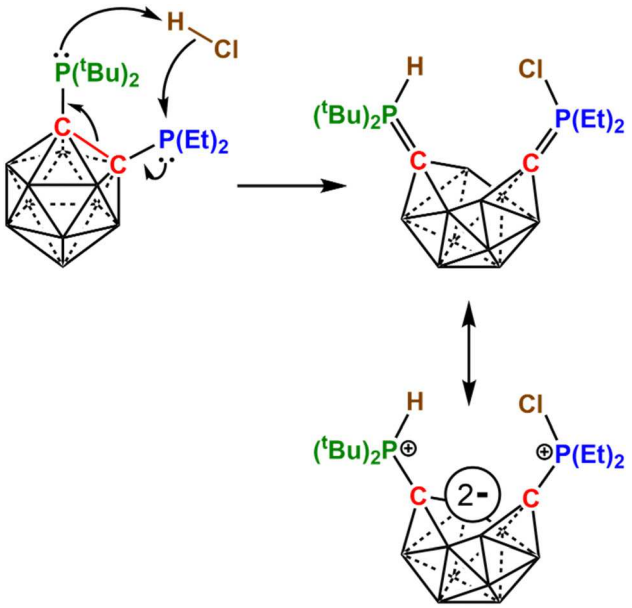

Fig. 2 Cage-opening reactivity of a carboranyl diphosphine with HCl.

demonstrated by the reaction of *ortho*-$C_2B_{10}H_{12}$ and magnesium metal in the presence of dibromoethane, which, upon workup, cleanly produces a different 7,10-$C_2B_{10}H_{13}^-$ cluster.[66,67]

This feature article will focus on the recent discoveries by our group and others pertinent to the electronic structure of *ortho*-$C_2B_{10}H_{12}$ clusters and the utilization of their redox properties in the metal-free activation of strong bonds as well as in ligand design.

Bond activations by carboranyl diphosphines

Conceptually, carboranyl diphosphines represent a molecular platform that merges two important features normally exhibited by transition metals with a relatively narrow HOMO–LUMO separation: the ability of the boron cluster to accept electrons and cycle through two-electron redox states, and the ability of the phosphine groups to donate electrons and provide binding sites. The resulting interplay between these two spatially separated fragments of the metal-free carboranyl diphosphine system opens a new reactivity manifold where coordination of a substrate and subsequent two-electron oxidative addition occur with the cleavage of substrate bonds.

The first example of the redox-active behavior of carboranyl diphosphines is the work of Pringle and co-workers.[68] The group synthesized a series of 1,2-{C_2B_{10}} diphosphines bearing various PR_2 groups at adjacent carbon atoms of the cluster, for example, *ortho*-1-P^{t}Bu$_2$-2-PEt$_2$-$C_2B_{10}H_{10}$. It was noted that the ^{31}P NMR spectrum of this compound in chloroform-*d* slowly changed upon standing for 28 days, with the appearance of two new singlets, one of which corresponded to the presence of a direct P–H bond. The crystal structure of the product revealed the cage-opening of the parent *closo*-{C_2B_{10}} cluster and its conversion to the *nido*-{C_2B_{10}} form. The more basic P^{t}Bu$_2$ group was selectively protonated in the product, and the PEt_2 group was converted to a PEt_2Cl fragment. This compound could also be directly obtained in the reaction of the starting carboranyl diphosphine and ethereal HCl (Fig. 2). Interestingly, the reverse reaction occurred easily upon the addition of triethylamine to the *nido*-{C_2B_{10}} product. The overall outcome of this reaction is therefore a formation of the zwitterionic product containing two phosphonium cations and the dianionic *nido*-{C_2B_{10}} cluster. The open cluster geometry was different from the previously reported *nido*-{C_2B_{10}} anions and can be described as a derivative of a C_2-symmetric 13-vertex docosahedron. Importantly, "regular" redox-inactive phosphines do not exhibit such reactivity with HCl, and instead become protonated at the phosphorus atom with the outer sphere halide counterion in the products.

The Hey-Hawkins group reported a related carboranyl diphosphetane that displays similar oxidative addition-type reactivity in the presence of MeI.[69] The synthesized carboranyl diphosphetane undergoes P–P bond activation and cluster opening upon reduction with lithium metal. The reaction of the resulting Li intermediate with excess MeI induces the methylation of both phosphorus centers, generating a zwitterionic bis-phosphonium-*nido*-carborane (Fig. 3). An attempt to obtain this open cluster compound though the direct reaction of the neutral diphosphine 1,2-(P^{t}BuMe)$_2$-$C_2B_{10}H_{10}$ with excess MeI resulted in the observed formation of the same product along with significant unidentified side products. It can be surmised that in order to form the diphosphonium zwitterion, the iodide counterions need to be oxidized by the cluster, generating I_2 and thus highlighting the key role of the carborane in this redox-active system.

These early examples, along with the findings of intramolecular bond activation in biscarboranyl phosphines (see the section below) inspired us to devise the system that would target metal-free reactivity driven by the redox rearrangement of the carborane cluster.

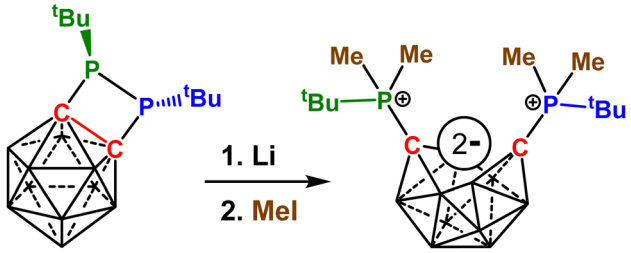

Fig. 3 Reaction of a carboranyl diphosphetane with MeI.

The targeted metal-free reactivity in main-group systems is based on the lowering in energy of the LUMO with the simultaneous maintenance or increase in energy of the HOMO. For carboranyl diphosphines, the HOMO can be envisioned to be centered on the phosphorus atoms, and therefore, an increase in the electron-donating abilities of the phosphine groups can be achieved by the utilization of alkyl substituents, such as *tert*-butyl or isopropyl groups. The LUMO is likely to be localized within the cluster; however, its energy is also governed by the conjugation with exohedral substituents. As mentioned in the introduction, the negative hyperconjugation between the lone pairs of the phosphine groups and the antibonding σ^*_{C-C} orbital within the *ortho*-carborane cluster can significantly increase the LUMO level, weakening the intracluster C–C bond and facilitating its opening upon reduction. Furthermore, the phosphine groups increase the steric encumbrance, thus contributing to the destabilization and lengthening of the intracluster C–C bond. Thus, in our work, we aimed to maximize both the electron-donating ability and the steric hindrance of the phosphine substituents on the *ortho*-carborane cluster.

A carborane bearing two electron-rich and sterically crowded phosphines, 1-P^{t}Bu$_2$-2-P^{i}Pr$_2$-C$_2$B$_{10}$H$_{10}$ (**1**), was obtained by stepwise deprotonation of the C–H bonds of *ortho*-C$_2$B$_{10}$H$_{12}$ and reactions with P^{t}Bu$_2$Cl and P^{i}Pr$_2$Cl, respectively (Fig. 4). The ^{31}P NMR spectrum of **1** contains two doublets with a large

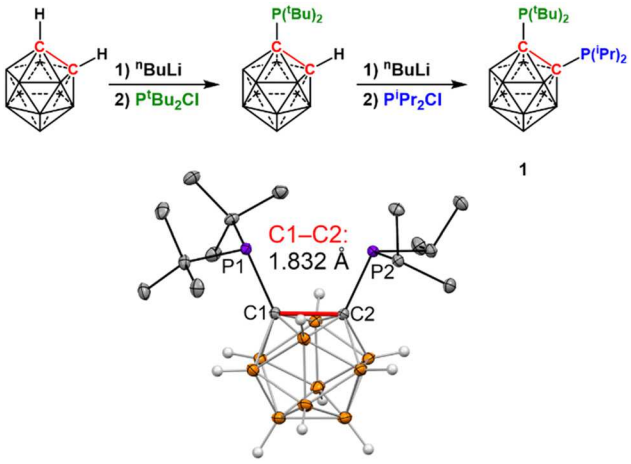

Fig. 4 Synthesis and displacement ellipsoid plot (50% probability) of **1**. Hydrogen atoms of alkyl groups are omitted for clarity.

coupling constant $^3J_{PP}$ = 90 Hz, indicating a strong through-bond interaction between phosphorus nuclei. The presence of two inequivalent phosphines in the molecule and their strong $^3J_{PP}$ coupling in the neutral *closo*- cluster was expected to be advantageous in exploring the redox reactivity of this compound. As shown below, the transformation of the *closo*-cluster to the *nido*- form upon reduction proceeds with the cleavage of the intracluster C–C bond and leads to the lack of appreciable coupling between the two inequivalent phosphorus nuclei, giving rise to a pair of singlets in ^{31}P NMR spectra. Single crystal X-ray diffraction confirmed the expected connectivity and revealed an intracluster carbon–carbon bond length of 1.832(2) Å, which is drastically longer than that of the unsubstituted *ortho*-C$_2$B$_{10}$H$_{12}$ cluster (1.624(8) Å)[70] and is the longest reported C–C distance for any carboranyl diphosphine.[71] This elongation was attributed to the aforementioned combination of the steric hindrance of the substituents as well as the electronic effects of the lone pairs of the electron-rich phosphine groups on the electron-accepting carborane cluster.

Theoretical calculations demonstrated that the HOMO and HOMO−1 of **1** are localized at the lone pairs on the phosphorus atoms, while the major components of the LUMO were the antibonding σ^*_{C-C} orbital and the bonding π_{C-P} orbitals, which supports the hypothesis that **1** is able to both efficiently donate electrons through the phosphine groups and accept electrons in the cluster, resulting in the cage opening and an increase in C–P bond order. Thus, the carboranyl diphosphine **1** can be considered as an ambiphilic molecule with spatially separated but conjugated electron-donating and electron-accepting regions.

We probed the redox behavior of **1** both chemically and electrochemically. Cyclic voltammograms of **1** exhibited quasi-irreversible overlapping reduction events with the position and peak shapes being solvent-dependent. Chemical reduction of **1** with sodium metal in THF resulted in the clean formation of a dianionic open cluster diphosphine **1**$^{2-}$, which was confirmed by NMR spectroscopy. Additionally, the structure of the reduced form of a congener of **1**, 1,2-(P^{i}Pr$_2$)$_2$-C$_2$B$_{10}$H$_{10}$, was determined by X-ray crystallography. Its crystal structure revealed the C_2-symmetric dianionic *nido*-{C$_2$B$_{10}$} cluster, isostructural to those reported in the Pringle and Hey-Hawkins works mentioned above.

This molecular design proved advantageous for the target metal-free bond activation reactivity. We found that **1** undergoes oxidative addition-type reactions with a rather broad range of substrates beyond just stronger electrophiles such as HCl and MeI. Reactions of **1** with main group hydrides, alcohols, and electron-deficient terminal alkynes resulted in generally similar oxidative addition-type *nido*-{C$_2$B$_{10}$} products – that is, the carborane cluster experienced a two-electron reduction with concurrent rupture of the intracluster C–C bond, and the phosphorus centers were converted to phosphonium cations *via* protonation or addition of substrate fragments.

For example, the reaction of **1** and tributylstannane proceeded cleanly to afford a single product according to ^{31}P{^{1}H} NMR spectroscopy. The most noticeable change in the NMR spectrum was the disappearance of the two doublet signals

from the inequivalent phosphine groups in **1** and the appearance of two new singlets. Furthermore, the proton-coupled ^{31}P NMR spectrum of the product contained two doublets ($^{1}J_{PH}$ of 432 and 437 Hz) corresponding to direct P–H bonds. The two-electron reduction of the *closo*-cluster to the *nido*-form and the simultaneous conversion of the phosphine groups into protonated phosphonium cations was accompanied by the formation of the tin–tin bond in the dimeric species $Bu_3Sn–SnBu_3$, the presence of which was confirmed with ^{119}Sn NMR spectroscopy. The crystal structure determination corroborated the spectral data and revealed the formation of a zwitterionic product featuring the open dianionic *nido*-{C_2B_{10}} cluster with its separated carbon atoms and protonated phosphonium centers (**2**) (Fig. 5). The open cluster exhibited the same C_2-symmetric geometry as that in the structure $\mathbf{1}^{2-}$. The exohedral bond lengths in **2** (1.747(1) Å and 1.751(1) Å), however, were significantly shorter that those in parent **1** (1.878(1) Å and 1.915(1) Å), which indicates their partial ylide character and corroborates the DFT calculation results described above.

The reactions of **1** with HBpin, NH_3BH_3, or $BH_3(SMe_2)$ produce the same open cluster **2**, albeit in lower yields (Fig. 5). Careful monitoring of the reaction progress between **1** and $BH_3(SMe_2)$ by ^{31}P NMR spectroscopy revealed the initial formation of two major open cluster products both containing P–H and P–B bonds, as evidenced by the presence of two pairs of sharp singlets and broad 1 : 1 : 1 : 1 quartets in the $^{31}P\{^{1}H\}$ NMR spectra of the reaction mixture. We were able to isolate and determine the crystal structure of one of these products, which featured the same open dianionic *nido*-{C_2B_{10}} cluster geometry along with a protonated H–P^{t}Bu$_2$ group and an (SMe$_2$)BH$_2$–P^{i}Pr$_2$ phospinoboryl group. This apparent product of the borane B–H bond activation by carboranyl diphosphine **1** eventually converts into **2** upon standing in solution. The reaction of **1** and ammonia borane required elevated temperatures to proceed and, along with the formation of **2**, was accompanied by the appearance of signals corresponding to oligomeric N–B containing products in the ^{11}B NMR spectrum.

Similar reactivity was observed in the activation of alcohols by **1**, producing P^{t}Bu$_2$(OR)-P^{i}Pr$_2$(H)-*nido*-$C_2B_{10}H_{10}$ (**3a** R = Me, **3b** R = ^{i}Pr). The reaction proceeded in the presence of an acid, suggesting that the protonation of one of the phosphine groups is an initial step. Interestingly, in the final products **3a**/**3b**, protonation occurs at the P^{i}Pr$_2$ group, and the more basic P^{t}Bu$_2$ group is connected to the alkoxide fragment. The cluster in **3a**/**3b** adopts the same open dianionic *nido*-{C_2B_{10}} geometry as in **2**.

A closely related example of bond activation by redox-active **1** was discovered in its reactions with alkynes.[72] We found that electron-deficient terminal alkynes were activated by our system in a process that is driven by cluster reduction and formation of the *nido*-{C_2B_{10}} cage, yet the products **4a**/**4b** did not follow the same reactivity pattern as the case described above (Fig. 6). Instead, the final outcome of the reaction is the regioselective activation of the B–H bond of the boron atom adjacent to both carbon atoms in the cluster. As a result, a boron–carbon bond is formed, and the alkyne fragment connects to the phosphorus atom of the P^{t}Bu$_2$ group, completing a

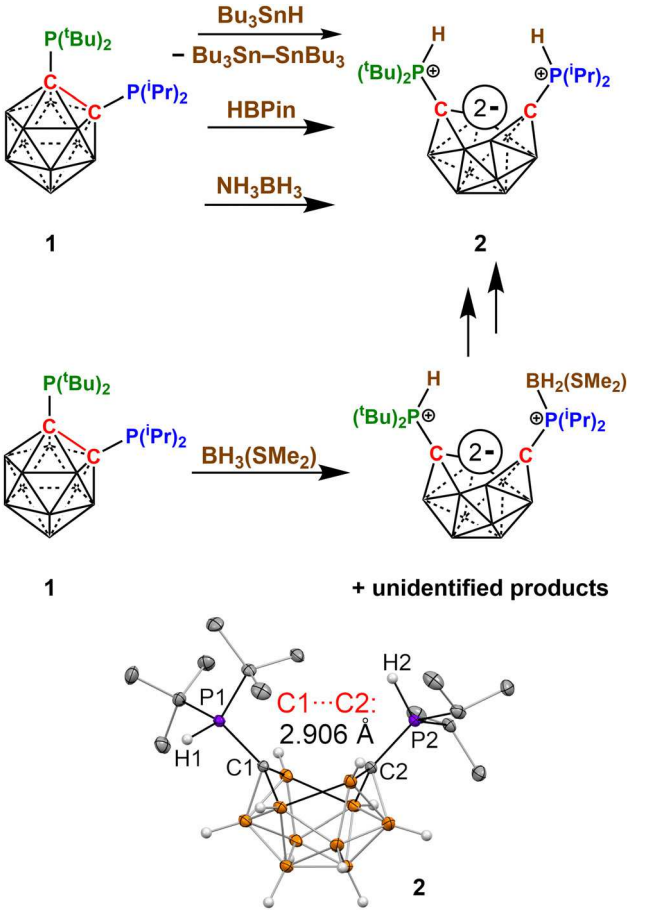

Fig. 5 Activation of main group hydrides by **1** (top) and displacement ellipsoid plot (50% probability) of **2** (bottom). Hydrogen atoms of alkyl groups are omitted for clarity.

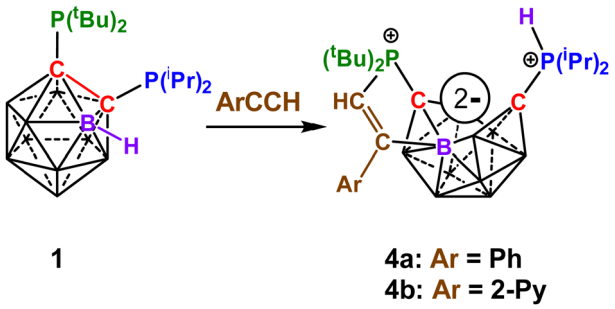

Fig. 6 Activation of electron-deficient terminal alkynes by **1**.

five-membered C–P–C(H)=C(Ar)–B cycle. The C–H bond of the terminal alkyne is retained, and the activated B–H bond of the cluster protonates the P^{i}Pr$_2$ group, as confirmed by deuterium labeling experiments. The transformation of the formally hydridic B–H bond into a proton provides two electrons for cluster reduction and opening. This cascading sequence of elementary steps creates a unique boron-containing cationic phosphacycle fused to the anionic *nido*-{C_2B_{10}} cluster. Importantly, the presence of the two phosphine groups is important for this

outcome, as carboranyl monophosphines do not exhibit B–H bond activation reactivity.[73,74]

To reiterate, the unusual reactivity of carboranyl diphosphine **1** described herein relies on the synergy between the electron-donating phosphine groups and the electron-accepting carborane cluster. In these novel transformations, the neutral *closo*-{C_2B_{10}} cluster accepts two electrons and becomes an open dianionic *nido*-{C_2B_{10}} cluster, while the two phosphine groups are converted into phosphonium cations. The resulting zwitterionic products exhibit ylide-type phosphorus-cluster bonding. Thus, the overall reactivity may be classified as the oxidative addition of substrates (*i.e.*, main group hydrides, alcohols, and electron-deficient terminal alkynes) to a carboranyl diphosphine.

Prior to our work with carboranyl diphosphine **1**, we observed intriguing reactivity while attempting to synthesize 1,1′-bis-*ortho*-carboranyl diphosphines. The structure of 1,1′-bis-*ortho*-carborane (“biscarborane”), similarly to biphenyl, features two carborane clusters joined together by a single carbon–carbon bond. In an attempt to obtain biscarboranyl diphosphines by deprotonation of two C–H bonds of biscarborane and a subsequent reaction with phosphine chlorides, we instead observed unprecedented regioselective cluster B–H activation at room temperature.[75] In retrospect, these transformations described below correspond to the promotion of intramolecular bond activation by a redox-active cluster, and are conceptually the same as the aforementioned examples of the reactivity of **1**.

Instead of the intended diphosphine, zwitterionic *closo*-{C_2B_{10}}-*nido*-{C_2B_{10}} clusters featuring an open *nido*-{C_2B_{10}} cluster and two phosphonium centers were isolated (Fig. 7). Both phosphorus atoms are connected to the carbon atoms of the biscarborane cage; therefore, one can assume that the installation of PR_2 groups to the cluster carbons indeed occurred in the initial stages of the reaction. However, the proximity of the phosphine substituents to the neighboring cluster evidently resulted in a transition state that corresponded to the close B–H···P contacts. The ensuing B–H bond activation is promoted by the *closo*-{C_2B_{10}} cluster accepting two electrons from the formally hydridic B–H bond and releasing a proton. The cluster is thus converted to the open dianionic *nido*-{C_2B_{10}} form, the P–B bond is formed, and the proton eventually migrates to the remaining neutral phosphine substituent, resulting in a protonated phosphonium cation. Importantly, the geometry of the *nido*-{C_2B_{10}} cluster is the same as for the zwitterionic products derived from **1** that are described above. Thus, the observed intramolecular B–H bond activation and the formation of a five membered C–C–B–P–C cycle is akin to the reactivity of **1** with alkynes.

Furthermore, our group has reported the ability of the zwitterionic compound *closo*-($C_2B_{10}H_{10}$)(P{N^{i}Pr$_2$}$_2$)-*nido*-($C_2B_{10}H_9$)-(PH{N^{i}Pr$_2$}$_2$) to activate the O–H bonds of water at room temperature, resulting in the partial removal of one boron and one carbon vertex from the *nido*-{C_2B_{10}} cluster and conversion to the *nido*-{CB_9} cage. This series of transformations culminates in the addition of H and OH fragments to separate sites of the molecule (Fig. 7).[76] While deboronation of carboranes is generally considered irreversible and requires external boron sources to reform the cluster, this reaction is reversible upon formal dehydration of the unusual boronic acid hydride (C)B(H)(OH) fragment at elevated temperatures, releasing water and rearranging to the starting *nido*-{C_2B_{10}} cage.

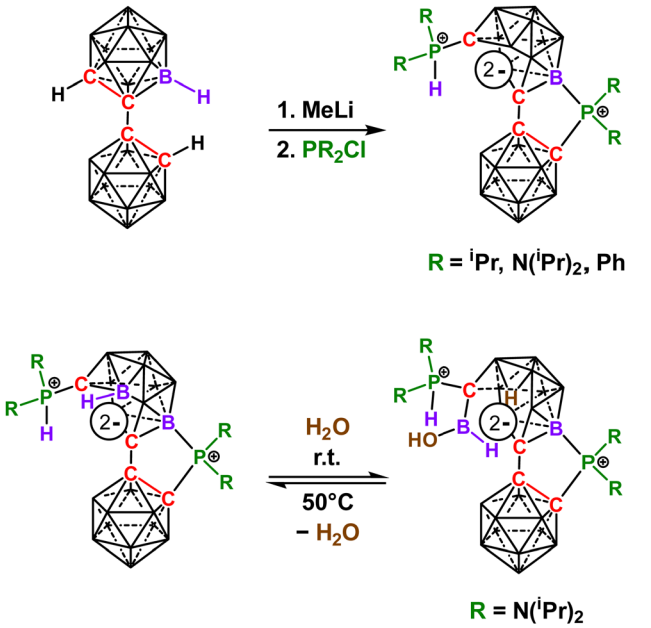

Fig. 7 Intramolecular B–H bond activation with biscarboranyl diphosphines.

Redox-active carboranes in the formation and stabilization of low-valent main group centers

In addition to facilitating the activation of strong bonds, carboranes in the pre-formed open *nido*-{C_2B_{10}} structure have also been employed in facilitating the formation and stabilization of unique main group centers. One such candidate for this design is a carborane cluster decorated with two intramolecularly donor-stabilized N-heterocyclic silylene (NHSi)[77] groups, **5**, which is isolobal to carboranyl diphosphines and is therefore able to accept and release electrons (Fig. 8).

Recently, Xie and co-workers have demonstrated a new method of direct borylene insertion into a B–H bond by employing **5** as a ligand.[78] The monobromoborylene **6** features a nucleophilic, electron-rich boron(I) center, stabilized by carborane-connected, strongly donating silylene groups. Upon reacting with sodium naphthalenide, **6** was shown to undergo the unprecedented insertion of a borylene fragment into a carborane cluster B–H bond, forming a new B–B bond. This unique reactivity is likely promoted by the electron-accepting propensity of the carborane cluster and the nucleophilicity of the borylene.

Mechanistic studies showed that an unstable carborane radical anion forms as a result of a one-electron reduction, promoting an intramolecular single-electron transfer from the

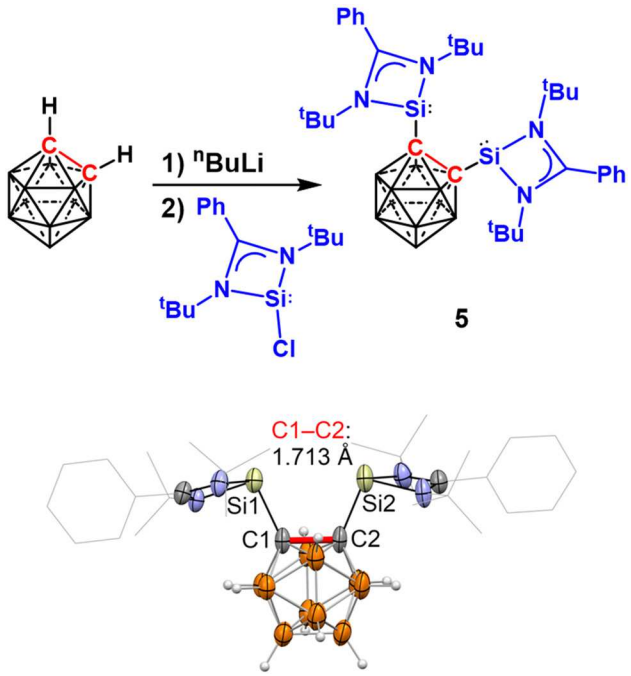

Fig. 8 Synthesis and displacement ellipsoid plot (50% probability) of **5**. Hydrogen atoms of alkyl and aryl groups are omitted for clarity.

boron(I) center to the carborane cluster. As a consequence, the more stable dianionic *nido*-{C_2B_{10}} cage and a boron-centered radical cation form (Fig. 9). During the reduction of the carborane cage, carbon–silicon bonds shorten, indicating a partial ylide character, analogous to the zwitterionic carboranyl diphosphines described in the previous section. Further reduction with sodium abstracts the bromide and creates an active borylene species, which then inserts into a B–H bond of the reduced cluster, creating a B–B bond. The capability of the carborane cluster to accept two electrons is crucial for this reactivity.

The ability of the carborane-linked bis-NHSi backbone **5** to reversibly accept and release electrons has also been applied to promote the formation and stabilization of low-valent compounds.

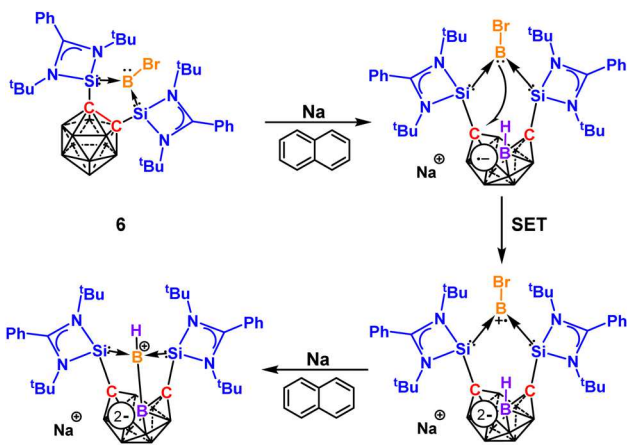

Fig. 9 Construction of B–B bond assisted by cage reduction.

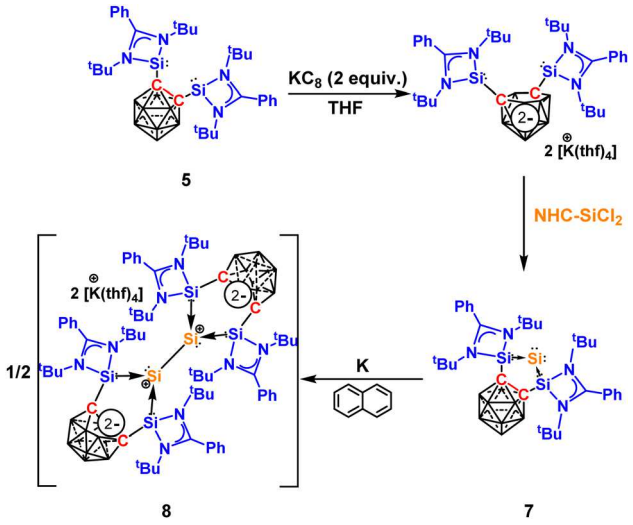

Fig. 10 Synthesis of silylone **7** *via* a dianionic *nido*-carboranyl bis-NHSi and the Si–Si homocoupling product **8**.

Driess and co-workers reported the ability of **5** to chelate and stabilize a zero-valent silicon center, named "silylone".[79] Similar to the aforementioned borylene insertion into a cluster B–H bond, the mechanism depends on the electron-accepting ability of the carborane cluster to facilitate electron transfer. Further reduction of silylone complex **7** leads to homocoupling and the formation of a low-valent Si(I)–Si(I) complex **8**, featuring two supporting dianionic *nido*-{C_2B_{10}} clusters (Fig. 10).

Stabilization of a monovalent nitrogen was also realized in a similar manner by Driess and co-workers (Fig. 11).[80] The reaction of **5** with adamantyl azide involves the reduction of the carborane cluster and the formation of silylene cations, generating zwitterionic product **9**.

The reduction of **9** with KC_8 in the presence of 18-crown-6 results in one-electron reduction and the loss of adamantyl and dinitrogen fragments to form a new anionic compound **10** (Fig. 12). The positive charge is localized at the nitrogen(I) center instead of the supporting silicon atoms, and the dinegative charge remains within the cluster, as indicated by the maintenance of a *nido*-{C_2B_{10}} geometry. The open cluster in **9** can be oxidized when reacted with AgOTf, which results in the formation of cationic compound **11**, with closure of the cluster, re-formation of the intracluster C–C bond, and loss of

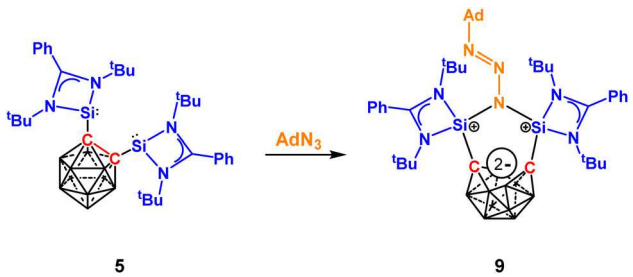

Fig. 11 Synthesis of *nido*-carboranyl bis-silylene-adamantyl azide adduct **9**.

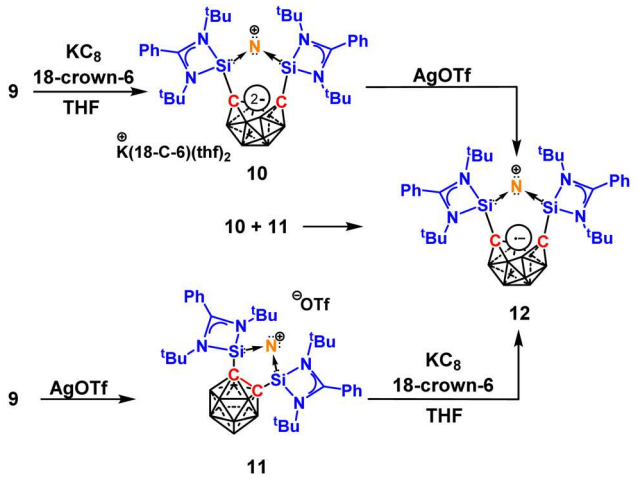

Fig. 12 Synthesis of low-valent nitrogen complexes **10** and **11** from **9** and the carborane-based radical nitrogen(I) species **12** from **10** and/or **11**.

dinitrogen and adamantyl fragments. The compounds **10** and **11** co-proportionate into a carborane-based radical species **12**.

Driess and co-workers recently reported the conceptually similar use of **5** in the synthesis of zero- and monovalent germanium species.[81] One-electron reduction of the zero-valent germanium(0) complex **13** was shown to induce an intramolecular electron transfer, reducing the carborane cluster by two electrons (exemplified by the transition from *closo*-$\{C_2B_{10}\}$ to the *nido*-$\{C_2B_{10}\}$ structure) and oxidizing the germanium center to Ge(I). This one-electron reduction, as with silylone **7**, facilitates Ge–Ge coupling to form a low-valent dimer complex **14**. Meanwhile, one-electron oxidation by ferrocenium forms a similar dicationic Ge(I)–Ge(I) complex **15** where both carborane clusters remain in the *closo*-form, thus not involving the redox properties of carborane for Ge(I) generation (Fig. 13).

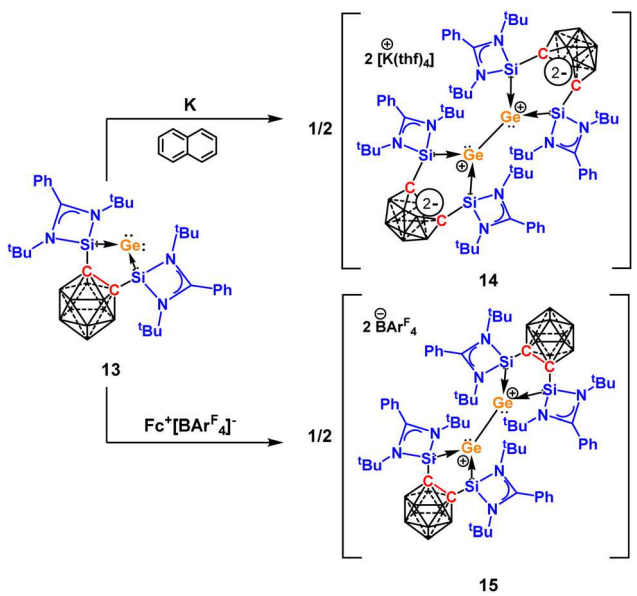

Fig. 13 Synthesis of Ge(I)–Ge(I) complexes **14** and **15** from germylone **13**.

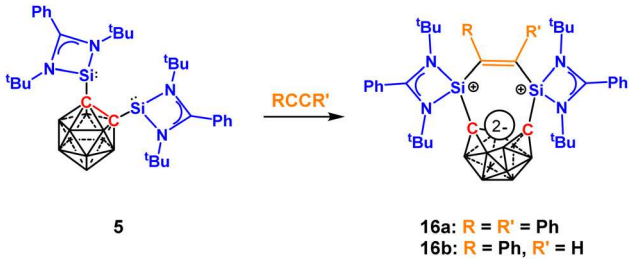

Fig. 14 Synthesis of the zwitterionic cyclic products **16a**/**16b**.

The carboranyl bis-NHSi ligand **5** was also employed in reactions with alkynes.[82] Treatment of **5** with either phenylacetylene or diphenylacetylene led to the formation of cyclic products **16a**/**16b** (Fig. 14), which features a C=C bridge between the two silicon centers and the open *nido*-$\{C_2B_{10}\}$ cluster. The exohedral C–Si bonds in **16a** are rather short (1.769(2) Å), which is consistent with its zwitterionic formulation. The geometry of the open cluster is analogous to that of **8**, **9**, **10**, **12**, and **14**.

The presence of the redox-active carborane cluster in the ligand backbone of **5** is integral to the formation of the aforementioned unique examples of low-valent Si, N, and Ge species. In most cases, the initial one-electron reduction of **5** drives the two-electron reduction of the carborane cluster, governed by the comparative stability of the dianionic *nido*-$\{C_2B_{10}\}$ cluster with respect to its radical monoanionic form; thus the second electron for the reduction of the cluster is sourced intramolecularly from the coordinated main group element center. For the germanium and silicon complexes, this results in the formation of Ge or Si radicals, which subsequently couple intermolecularly to form their respective dimers. For the low-valent nitrogen complex, this one-electron intramolecular oxidation results in the fragmentation of the adamantyl azide moiety and the formation of the nitrogen(I) cation.

Redox-active carboranes as supporting ligands for transition metals

C–C bond activation with metallacarboranes

The activation of C–C bonds often requires the involvement of transition metal catalysts. Among different classes of organic compounds, aromatic carbon–carbon bonds are some of the most stable and most challenging for activation. Welch and co-workers have reported an interesting example of aromatic C–C bond cleavage in a simple arene at room temperature by a metallacarborane complex.[83]

The reduction of the biscarborane cluster with excess lithium metal and the subsequent reaction with [(*p*-cymene)-$RuCl_2]_2$ failed to produce the intended C–C bridged bis-13-vertex metallacarborane. Instead, only one cluster of biscarborane was expanded with the metal vertex, producing an $\{RuC_2B_{10}\}$ cluster. Surprisingly, a triple-decker "fly-over bridge" bimetallic complex formed, with the rupture of the C–C bond in one of initial *p*-cymene ligands (Fig. 15). The results of DFT calculations

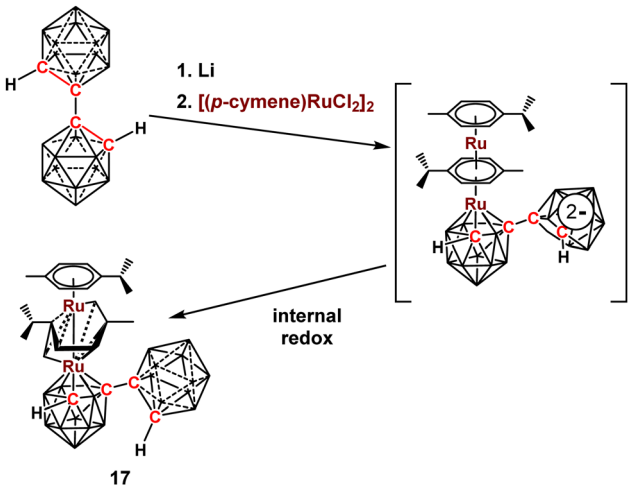

Fig. 15 Synthesis of fly-over bridge complex **17**.

suggest that the mechanism of the aromatic C–C bond activation involves an intramolecular electron transfer from the reduced pendant carborane cluster to the coordinated arene ligand. This discovery highlights the role of the carborane cluster as an electron reservoir for a subsequent redox process at a remote metal site.

Change of ligand coordination mode

Ménard, Dobrovetsky, Hayton, and co-workers recently illustrated the novel use of a carborane-based ligand for the capture and release of uranium in the form of UO_2^{2+}.[84] Reduction of neutral 1,2-$(Ph_2PO)_2$-1,2-*closo*-$C_2B_{10}H_{10}$ by two electrons leads the formation of the dianionic *nido*-$\{C_2B_{10}\}$ cluster. This cage opening upon reduction leads to a significant increase in the geometrical separation of the exohedral phosphine oxide binding sites, thus dramatically changing the bite angle of this ligand. This increased bite angle facilitates its coordination to the large uranyl cation. Once coordinated, the UO_2^{2+} fragment can be effectively released through oxidation, converting the cluster backbone of the ligand back to the *closo*-form and decreasing the bite angle (Fig. 16). This reaction proceeds reversibly *via* the chemical or electrochemical reduction of the carborane compound, making this a controllable redox cycle. This development has substantial potential in the processing and separation of nuclear fuel waste. Both neutral and dianionic forms of the ligand are stable in the presence of water and thus the concept of geometric changes driven by the redox cycling of carboranyl ligands has been extended to the selective biphasic extraction and release of uranyl.[85]

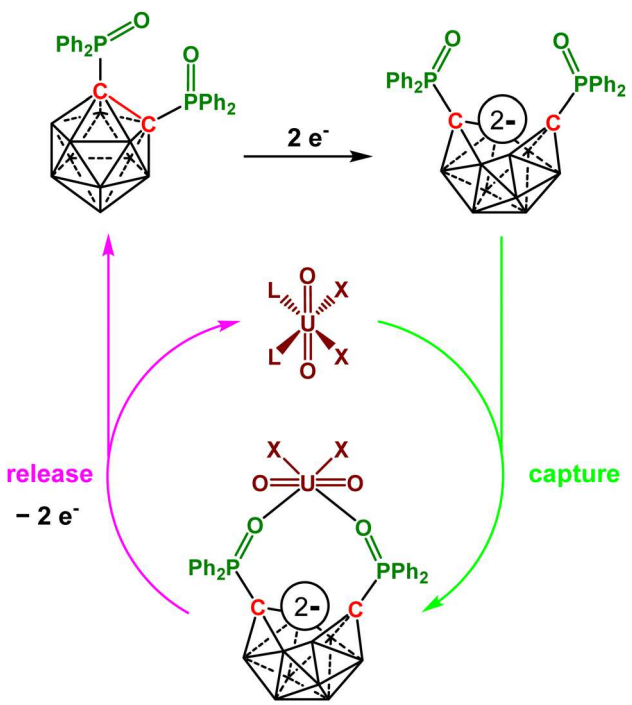

Fig. 16 Capture and release of UO_2^{2+} by a redox-active carborane derivative.

Conclusions and outlook

The findings summarized in this feature article put forward a new mode of metal-free bond activation reactions by main group cluster systems. The 3D aromaticity and electronic properties of carboranes, as well as the influence of exohedral substituents, have been investigated and harnessed since the discovery of these intriguing clusters. The reversible redox transformations of carborane clusters have proven to be a tool for a diverse range of applications, as exemplified by the reactivity discussed in this article. The tunability of these cluster compounds through exohedral substitution will likely lead to new bond activation discoveries as even subtle changes in the substituents can have a profound impact on the reactivity. The electron-accepting ability of the icosahedral carborane cluster can be used to facilitate metal-free reactivity by inducing a transition from the neutral *closo*-$\{C_2B_{10}\}$ to the dianionic *nido*-$\{C_2B_{10}\}$ structure. Furthermore, the redox properties of the cluster could be utilized in an indirect way, as the geometric changes associated with the opening of the cluster upon reduction can be used to alter its coordination chemistry.

Conflicts of interest

There are no conflicts to declare.

Acknowledgements

This material is based upon work supported by the National Science Foundation under grant CHE-2154828.

Notes and references

1 R. H. Crabtree, *The Organometallic Chemistry of the Transition Metals*, Wiley, Hoboken, NJ, 7th edition., 2019.
2 P. P. Power, *Nature*, 2010, **463**, 171–177.
3 D. Martin, M. Soleilhavoup and G. Bertrand, *Chem. Sci.*, 2011, **2**, 389–399.
4 D. W. Stephan, *Chem*, 2020, **6**, 1520–1526.

5 M.-A. Légaré, C. Pranckevicius and H. Braunschweig, *Chem. Rev.*, 2019, **119**, 8231–8261.
6 N. L. Dunn, M. Ha and A. T. Radosevich, *J. Am. Chem. Soc.*, 2012, **134**, 11330–11333.
7 F.-G. Fontaine and É. Rochette, *Acc. Chem. Res.*, 2018, **51**, 454–464.
8 M. Karimi, R. Borthakur, C. L. Dorsey, C.-H. Chen, S. Lajeune and F. P. Gabbaï, *J. Am. Chem. Soc.*, 2020, **142**, 13651–13656.
9 L. Liu, L. L. Cao, Y. Shao, G. Ménard and D. W. Stephan, *Chem*, 2017, **3**, 259–267.
10 T. Chu and G. I. Nikonov, *Chem. Rev.*, 2018, **118**, 3608–3680.
11 Y. Su and R. Kinjo, *Chem. Soc. Rev.*, 2019, **48**, 3613–3659.
12 T. J. Hadlington, M. Driess and C. Jones, *Chem. Soc. Rev.*, 2018, **47**, 4176–4197.
13 C. Weetman and S. Inoue, *ChemCatChem*, 2018, **10**, 4213–4228.
14 R. L. Melen, *Science*, 2019, **363**, 479–484.
15 J. M. Lipshultz, G. Li and A. T. Radosevich, *J. Am. Chem. Soc.*, 2021, **143**, 1699–1721.
16 M. F. Cain, *Comments Inorg. Chem.*, 2020, **40**, 25–51.
17 J. S. Jones and F. P. Gabbaï, *Acc. Chem. Res.*, 2016, **49**, 857–867.
18 J. M. Bayne and D. W. Stephan, *Chem. Soc. Rev.*, 2016, **45**, 765–774.
19 J. Abbenseth and J. M. Goicoechea, *Chem. Sci.*, 2020, **11**, 9728–9740.
20 G. D. Frey, V. Lavallo, B. Donnadieu, W. W. Schoeller and G. Bertrand, *Science*, 2007, **316**, 439–441.
21 G. D. Frey, J. D. Masuda, B. Donnadieu and G. Bertrand, *Angew. Chem., Int. Ed.*, 2010, **49**, 9444–9447.
22 S. Lim and A. T. Radosevich, *J. Am. Chem. Soc.*, 2020, **142**, 16188–16193.
23 W. Zhao, S. M. McCarthy, T. Y. Lai, H. P. Yennawar and A. T. Radosevich, *J. Am. Chem. Soc.*, 2014, **136**, 17634–17644.
24 K. Chulsky, I. Malahov, D. Bawari and R. Dobrovetsky, *J. Am. Chem. Soc.*, 2023, **145**, 3786–3794.
25 R. N. Grimes, *Carboranes*, Academic Press, Amersterdam; Boston, 3 edition., 2016.
26 M. F. Hawthorne, *Boranes and Beyond: History and the Man Who Created Them*, Springer, New York, NY, 2023.
27 Z. Chen and R. B. King, *Chem. Rev.*, 2005, **105**, 3613–3642.
28 J. Poater, M. Solà, C. Viñas and F. Teixidor, *Angew. Chem., Int. Ed.*, 2014, **53**, 12191–12195.
29 J. Poater, C. Viñas, I. Bennour, S. Escayola, M. Solà and F. Teixidor, *J. Am. Chem. Soc.*, 2020, **142**, 9396–9407.
30 R. N. Grimes, *Dalton Trans.*, 2015, **44**, 5939–5956.
31 J. M. Stauber, E. A. Qian, Y. Han, A. L. Rheingold, P. Král, D. Fujita and A. M. Spokoyny, *J. Am. Chem. Soc.*, 2020, **142**, 327–334.
32 A. B. Buades, V. Sanchez Arderiu, D. Olid-Britos, C. Viñas, R. Sillanpää, M. Haukka, X. Fontrodona, M. Paradinas, C. Ocal and F. Teixidor, *J. Am. Chem. Soc.*, 2018, **140**, 2957–2970.
33 S. P. Fisher, A. W. Tomich, S. O. Lovera, J. F. Kleinsasser, J. Guo, M. J. Asay, H. M. Nelson and V. Lavallo, *Chem. Rev.*, 2019, **119**, 8262–8290.
34 J. C. Axtell, L. M. A. Saleh, E. A. Qian, A. I. Wixtrom and A. M. Spokoyny, *Inorg. Chem.*, 2018, **57**, 2333–2350.
35 S. P. Fisher, A. W. Tomich, J. Guo and V. Lavallo, *Chem. Commun.*, 2019, **55**, 1684–1701.
36 P. Stockmann, M. Gozzi, R. Kuhnert, M. B. Sárosi and E. Hey-Hawkins, *Chem. Soc. Rev.*, 2019, **48**, 3497–3512.
37 Y. Quan and Z. Xie, *Chem. Soc. Rev.*, 2019, **48**, 3660–3673.
38 R. Frank, V. Ahrens, S. Boehnke, S. Hofmann, M. Kellert, S. Saretz, S. Pandey, M. Sárosi, Á. Bartók, A. G. Beck-Sickinger and E. Hey-Hawkins, *Pure Appl. Chem.*, 2015, **87**, 163–171.
39 A. Saha, E. Oleshkevich, C. Vinas and F. Teixidor, *Adv. Mater.*, 2017, **29**, 1704238.
40 F. Lerouge, A. Ferrer-Ugalde, C. Viñas, F. Teixidor, R. Sillanpää, A. Abreu, E. Xochitiotzi, N. Farfán, R. Santillan and R. Núñez, *Dalton Trans.*, 2011, **40**, 7541–7550.
41 B. J. Eleazer and D. V. Peryshkov, *Comments Inorg. Chem.*, 2018, **38**, 79–109.
42 M. Scholz and E. Hey-Hawkins, *Chem. Rev.*, 2011, **111**, 7035–7062.
43 J. Poater, C. Viñas, M. Solà and F. Teixidor, *Nat. Commun.*, 2022, **13**, 3844.
44 F. Sun, S. Tan, H.-J. Cao, C. Lu, D. Tu, J. Poater, M. Solà and H. Yan, *J. Am. Chem. Soc.*, 2023, **145**, 3577–3587.
45 K. P. Anderson, H. A. Mills, C. Mao, K. O. Kirlikovali, J. C. Axtell, A. L. Rheingold and A. M. Spokoyny, *Tetrahedron*, 2019, **75**, 187–191.
46 H. D. A. C. Jayaweera, M. M. Rahman, P. J. Pellechia, M. D. Smith and D. V. Peryshkov, *Chem. Sci.*, 2021, **12**, 10441–10447.
47 C. Vinas, R. Benakki, F. Teixidor and J. Casabo, *Inorg. Chem.*, 1995, **34**, 3844–3845.
48 A.-R. Popescu, A. D. Musteti, A. Ferrer-Ugalde, C. Viñas, R. Núñez and F. Teixidor, *Chem. – Eur. J.*, 2012, **18**, 3174–3184.
49 A. V. Puga, F. Teixidor, R. Sillanpää, R. Kivekäs, M. Arca, G. Barberà and C. Viñas, *Chem. – Eur. J.*, 2009, **15**, 9755–9763.
50 L. A. Boyd, W. Clegg, R. C. B. Copley, M. G. Davidson, M. A. Fox, T. G. Hibbert, J. A. K. Howard, A. Mackinnon, R. J. Peace and K. Wade, *Dalton Trans.*, 2004, 2786–2799.
51 M. A. Fox, R. J. Peace, W. Clegg, M. R. J. Elsegood and K. Wade, *Polyhedron*, 2009, **28**, 2359–2370.
52 Z. Kelemen, A. Pepiol, M. Lupu, R. Sillanpää, M. M. Hänninen, F. Teixidor and C. Viñas, *Chem. Commun.*, 2019, **55**, 8927–8930.
53 J. M. Oliva, N. L. Allan, P. V. R. Schleyer, C. Viñas and F. Teixidor, *J. Am. Chem. Soc.*, 2005, **127**, 13538–13547.
54 R. Pang, J. Li, Z. Cui, C. Zheng, Z. Li, W. Chen, F. Qi, L. Su and X.-Q. Xiao, *Dalton Trans.*, 2019, **48**, 7242–7248.
55 J. Li, R. Pang, Z. Li, G. Lai, X.-Q. Xiao and T. Müller, *Angew. Chem., Int. Ed.*, 2019, **58**, 1397–1401.
56 N. Mandal and A. Datta, *Chem. Commun.*, 2020, **56**, 15377–15386.
57 G. B. Dunks, R. J. Wiersema and M. F. Hawthorne, *J. Am. Chem. Soc.*, 1973, **95**, 3174–3179.
58 R. Núñez, M. Tarrés, A. Ferrer-Ugalde, F. F. de Biani and F. Teixidor, *Chem. Rev.*, 2016, **116**, 14307–14378.
59 J. R. Miller, A. R. Cook, L. Šimková, L. Pospíšil, J. Ludvík and J. Michl, *J. Phys. Chem. B*, 2019, **123**, 9668–9676.
60 L. Weber, J. Kahlert, L. Böhling, A. Brockhinke, H.-G. Stammler, B. Neumann, R. A. Harder, P. J. Low and M. A. Fox, *Dalton Trans.*, 2013, **42**, 2266–2281.
61 J. Kahlert, L. Böhling, A. Brockhinke, H.-G. Stammler, B. Neumann, L. M. Rendina, P. J. Low, L. Weber and M. A. Fox, *Dalton Trans.*, 2015, **44**, 9766–9781.
62 T. D. Getman, C. B. Knobler and M. F. Hawthorne, *J. Am. Chem. Soc.*, 1990, **112**, 4593–4594.
63 T. D. Getman, C. B. Knobler and M. F. Hawthorne, *Inorg. Chem.*, 1992, **31**, 101–105.
64 D. McKay, S. A. Macgregor and A. J. Welch, *Chem. Sci.*, 2015, **6**, 3117–3128.
65 G. B. Gange, A. L. Humphries, D. E. Royzman, M. D. Smith and D. V. Peryshkov, *J. Am. Chem. Soc.*, 2021, **143**, 10842–10846.
66 C. Viñas, G. Barberà and F. Teixidor, *J. Organomet. Chem.*, 2002, **642**, 16–19.
67 J. Bould, A. Laromaine, C. Viñas, F. Teixidor, L. Barton, N. P. Rath, R. E. K. Winter, R. Kivekäs and R. Sillanpää, *Organometallics*, 2004, **23**, 3335–3342.
68 J. P. H. Charmant, M. F. Haddow, R. Mistry, N. C. Norman, A. G. Orpen and P. G. Pringle, *Dalton Trans.*, 2008, 1409–1411.
69 J. Schulz, A. Kreienbrink, P. Coburger, B. Schwarze, T. Grell, P. Lönnecke and E. Hey-Hawkins, *Chem. – Eur. J.*, 2018, **24**, 6208–6216.
70 A. R. Turner, H. E. Robertson, K. B. Borisenko, D. W. H. Rankin and M. A. Fox, *Dalton Trans.*, 2005, 1310–1318.
71 A. R. Popescu, F. Teixidor and C. Viñas, *Coord. Chem. Rev.*, 2014, **269**, 54–84.
72 G. B. Gange, A. L. Humphries, M. D. Smith and D. V. Peryshkov, *Inorg. Chem.*, 2022, **61**, 18568–18573.
73 F. Zheng, T.-F. Leung, K.-W. Chan, H. H. Y. Sung, I. D. Williams, Z. Xie and G. Jia, *Chem. Commun.*, 2016, **52**, 10767–10770.
74 G. Tao, M. Bai, Z. Liu and Z. Duan, *Organometallics*, 2021, **40**, 4041–4044.
75 Y. O. Wong, M. D. Smith and D. V. Peryshkov, *Chem. – Eur. J.*, 2016, **22**, 6764–6767.
76 Y. O. Wong, M. D. Smith and D. V. Peryshkov, *Chem. Commun.*, 2016, **52**, 12710–12713.
77 C.-W. So, H. W. Roesky, J. Magull and R. B. Ostwald, *Angew. Chem., Int. Ed.*, 2006, **45**, 3948–3950.
78 H. Wang, J. Zhang, H. K. Lee and Z. Xie, *J. Am. Chem. Soc.*, 2018, **140**, 3888–3891.
79 S. Yao, A. Kostenko, Y. Xiong, A. Ruzicka and M. Driess, *J. Am. Chem. Soc.*, 2020, **142**, 12608–12612.
80 S. Yao, T. Szilvási, Y. Xiong, C. Lorent, A. Ruzicka and M. Driess, *Angew. Chem., Int. Ed.*, 2020, **59**, 22043–22047.
81 S. Yao, A. Kostenko, Y. Xiong, C. Lorent, A. Ruzicka and M. Driess, *Angew. Chem., Int. Ed.*, 2021, **60**, 14864–14868.

82 R. Liu, Y. Tang, C. Wang, Z.-F. Zhang, M.-D. Su and Y. Li, *Inorg. Chem.*, 2023, **62**, 1095–1101.
83 D. Ellis, D. McKay, S. A. Macgregor, G. M. Rosair and A. J. Welch, *Angew. Chem., Int. Ed.*, 2010, **49**, 4943–4945.
84 M. Keener, C. Hunt, T. G. Carroll, V. Kampel, R. Dobrovetsky, T. W. Hayton and G. Ménard, *Nature*, 2020, **577**, 652–655.
85 M. Keener, M. Mattejat, S.-L. Zheng, G. Wu, T. W. Hayton and G. Ménard, *Chem. Sci.*, 2022, **13**, 3369–3374.